Molecular Therapy
Methods & Clinical Development
Original Article

Characterization of AAV-mediated dorsal root ganglionopathy

Nicholas Buss,[1] Lisa Lanigan,[2] Jillynne Zeller,[3] Derek Cissell,[4] Monica Metea,[5] Eric Adams,[2] Mikayla Higgins,[1] Kwi Hye Kim,[1] Ewa Budzynski,[1] Lin Yang,[1] Ye Liu,[1] Mark Butt,[2] Olivier Danos,[1] and Michele Fiscella[1]

[1]REGENXBIO, Rockville, MD 20850, USA; [2]StageBio, Frederick, MD 21701, USA; [3]Northern Biomedical Research, Spring Lake, MI 49456, USA; [4]Invicro, Needham, MA 02494, USA; [5]Preclinical Electrophysiology Consulting, Mattapoisett, MA 02739, USA

Recent studies in non-human primates administered recombinant adeno-associated viruses (rAAVs) have shown lesions in the dorsal root ganglia (DRG) of unknown pathogenesis. In this study, rAAV9s manufactured using different purification methods alongside a non-expressing Null AAV9 vector was administered to groups of cynomolgus monkeys followed by neuropathological evaluation after 4 weeks. Lesions, including neuronal degeneration, increased cellularity, and nerve fiber degeneration, were observed in the DRG, regardless of purification methods. Animals did not develop any neurological signs throughout the study, and there was no loss of function observed in neuro-electrophysiological endpoints or clear effects on intraepidermal nerve fiber density. However, magnetic resonance imaging (MRI) of animals with axonopathy showed an increase in short tau inversion recovery (STIR) intensity and decrease in fractional anisotropy. In animals administered the Null AAV9 vector, DRG lesions were not observed despite vector DNA being detected in the DRG at levels equivalent to or greater than rAAV9-treated animals. This study further supports that DRG toxicity is associated with transgene overexpression in DRGs, with particular sensitivity at the lumbar and lumbosacral level. The data from this study also showed that the nerve fiber degeneration did not correlate with any functional effect on nerve conduction but was detectable by MRI.

INTRODUCTION

Recombinant adeno-associated viruses (rAAVs) are becoming an established therapeutic modality for delivery of gene therapies, as shown by the recent approval of two AAV-based gene therapies and the number of clinical trials currently being conducted.[1] Delivery of AAVs to the central nervous system (CNS) to treat various neurological disorders has been shown to be effective in preclinical studies, and clinical trials are ongoing for many diseases, including mucopolysaccharidoses (MPSs), neuronal ceroid lipofuscinoses (NCLs), spinal muscular atrophy (SMA), and giant axonal neuropathy.[2] While emerging clinical data from these trials are encouraging, degeneration of dorsal root ganglia (DRG) neurons has been described in some non-human primates (NHPs) studies following administration of rAAVs.[3–7] The etiology, pathogenesis, and clinical relevance of these findings are not fully understood and have not been consistently reported.[8,9] Furthermore, a 4-year study following intrathecal administration of AAV9.hIDUA to juvenile NHPs did not report DRG pathology, suggesting that either toxicity does not affect young animals or that the initial morphological changes resolve over time.[10] The cause of dorsal root ganglionopathy is unknown, but current hypotheses include either an immune response to the capsid or transgene product, protein overexpression, or vector quality, including varying levels of empty and full capsids that are generally dependent on the purification processes used.

In this study, we administered different preparations of rAAV9s into the cisterna magna of NHPs, including a vector not expressing any transgene mRNA (Null), to evaluate the vector characteristics that may be associated with the DRG toxicity over 4 weeks. We also performed a comprehensive functional assessment of nerve conduction (neuro-electrophysiology) as well as an assessment of intraepidermal nerve fiber density (IENFD) and magnetic resonance imaging (MRI) of the spinal regions of interest (lumbar and lumbosacral region) where these changes have been observed. These represent measurable and translatable safety endpoints to use in the clinic for monitoring of subjects treated with these gene therapies.

RESULTS

Vector preparations

AAV9.hCLN2 vector (see materials and methods) was prepared using three different purification processes known to yield different percentages of full, partial, or empty capsids: anion exchange chromatography alone (AEX), cation exchange chromatography (CEX) prior to AEX, or ultracentrifugation (UC) prior to AEX. Following these purification steps, the preparations were subjected to analytical ultracentrifugation to determine the percent of full, partial, or empty capsids. As expected, the percentage of full capsids present in the final preparations increased with the additional purification steps, from 74.1% for AEX to 86.3% and 95.5% for CEX and UC, respectively

Received 30 November 2021; accepted 27 January 2022;
https://doi.org/10.1016/j.omtm.2022.01.013.

Correspondence: Nicholas Buss, PhD, REGENXBIO, 9804 Medical Center Drive, Rockville, MD 20850, USA.
E-mail: nbuss@regenxbio.com

Table 1. Study design

Group	Test article	Analytical ultracentrifugation (%)			Dose (GC/animal)	Vector genome concentration (GC/mL)[a]	Animal number	
		Full capsid	Partial capsids	Empty capsids			Male	Female
1	vehicle	–	–	–	0	0	1, 2	13, 14
2	AAV9.hCLN2-AEX	74.1	6.8	19.0	3.1×10^{13}	3.1×10^{13}	3, 4	15A, 16
3	AAV9.hCLN2-CEX	86.3	7.0	6.7	3.1×10^{13}	3.1×10^{13}	5, 6	17, 18
4	AAV9.hCLN2-UC	95.5	3.8	0.6	3.1×10^{13}	3.1×10^{13}	7, 8	19, 20
5	AAV9.hCLN2-AEX	NT	NT	NT	1.1×10^{14}	1.1×10^{14}	9A, 10	21, 22
6	AAV9.Null[b]	70.8	NT	NT	2.8×10^{13}	2.8×10^{13}	011, 12	23, 24

All test articles met the endotoxin and bioburden acceptance criteria of $\leq$0.5 endotoxin units (EU)/mL and $\leq$10 colony-forming units (CFUs)/1 mL, respectively. Potency was assessed using a HEK293 transduction/TPP1 enzymatic activity assay and was comparable for all test articles. The stability results indicate the test and control articles remained stable for the duration of use in the nonclinical study (Table S1). The in-use stability results indicate that AAV9.hCLN2 is stable for up to 6 h at room temperature. In addition, it was demonstrated that AAV9.hCLN2 is compatible with the delivery devices used for intracisternal administration. AEX, anion exchange chromatography; CEX, cation exchange chromatography; NT, not tested; UC, ultracentrifugation.

[a]Vector genome concentration determined using ddPCR

[b]AAV9.Null was purified by AEX

(Table 1). The AAV9.Null vector (see materials and methods) was purified by AEX with 70.8% full capsids (Table 1).

In-life assessment

Groups of cynomolgus monkeys (2/sex/group) were administered a single dose of either vehicle (control group) or different preparations and doses of AAV9.hCLN2 or AAV9.Null vector via cisterna magna puncture (1 mL/animal) to investigate the toxicity of the test articles over 4 weeks (see Table 1 for study design). During this study, endpoints included clinical observations, body weight, food consumption, pharmacodynamics (transgene expression as determined by tripeptidyl peptidase 1 [TPP1] concentration), immunogenicity (anti-AAV9 neutralizing antibodies [NAbs] and anti-TPP1 antibodies), biodistribution, organ weights, and macroscopic and microscopic examination. During the study, there were no test-article-related clinical observations or effects on body weight or food intake in animals receiving AAV9.hCLN2 or AAV9.Null vectors. Prior to dosing, all animals were negative for the presence of anti-AAV9 with the exception of one male and one female (titers of five and three, respectively) in the group administered AAV9.hCLN2-CEX. This positivity did not appear to impact tissue biodistribution when compared with the other two animals in this group (Figures S4 and S5).

Biodistribution, pharmacodynamics, and immunogenicity

Administration of AAV9.hCLN2 into the cisterna magna led to widespread biodistribution in all regions of the brain, both deep and superficial layers. There were differences within regions of the brain, with lower levels detected within the striatum and thalamus when compared with other brain regions (Figure S1). In general, there were no clear differences in biodistribution between AAV9.hCLN2 purification processes, although a trend for higher levels of vector DNA was seen in the group receiving AAV9.hCLN2-UC (Figure S1). For AAV9.hCLN2-AEX administered at two dose levels of either 3.1×10^{13} or 1.1×10^{14} genome copies (GC)/animal, dose-related increases in mean vector DNA were observed in most regions, except striatum (deep) and cerebellum (superficial; Figure S1). Vector DNA was detected in the sciatic nerve (proximal), spinal cord, and DRG at the cervical, thoracic, and lumbar level, with vector DNA at the highest levels at the lumbar DRG for animals that were administered AAV9.hCLN2 (Figure S2). For animals that were administered AAV9.Null, vector DNA was detected in all regions of the brain, spinal cord, and, importantly, DRG (cervical, thoracic, and lumbar) at similar or greater levels than those seen with AAV9.hCLN2-treated cynomolgus monkeys (Figure S2). Peripheral vector DNA biodistribution was also seen in the lymph nodes, heart, kidney, liver, lung, and gonads (Figure S3). The lack of vector DNA detected in the testes of both males given the high dose of AAV9.hCLN2-AEX is of unknown relevance based on the number of animals and age range used. With respect to transgene expression, TPP1 concentration in AAV9.hCLN2-treated animals showed increases above endogenous TPP1 in cerebrospinal fluid (CSF) and serum. Anti-transgene product antibodies (ATPAs) were detected in serum of all animals in groups administered AAV9.hCLN2, which was associated with a decrease in TPP1 concentration in serum and CSF by day 30 (Figures S6 and S7). On day 15, TPP1 concentrations in the serum were generally comparable between AAV9.hCLN2 purification processes. There were some differences noted between vector preparations in CSF TPP1 concentration on day 15, with UC greater than AEX and AEX greater than CEX, but due to the limited number of animals and that anti-TPP1 antibodies observed likely influenced both CSF and serum TPP1 concentrations on day 30, the relevance of this observation is unknown.

In animals administered with AAV9.Null vector, as expected, TPP1 concentrations were comparable to those in control animals throughout the study in the serum and CSF.

At the end of the study, all animals administered rAAV9s developed similar post-dose serum anti-AAV9 NAbs titers (titers ranging from 20 to 4,374), indicating similar immunogenicity of the various rAAV9 preparations and the AAV9.Null (Figures S8 and S9).

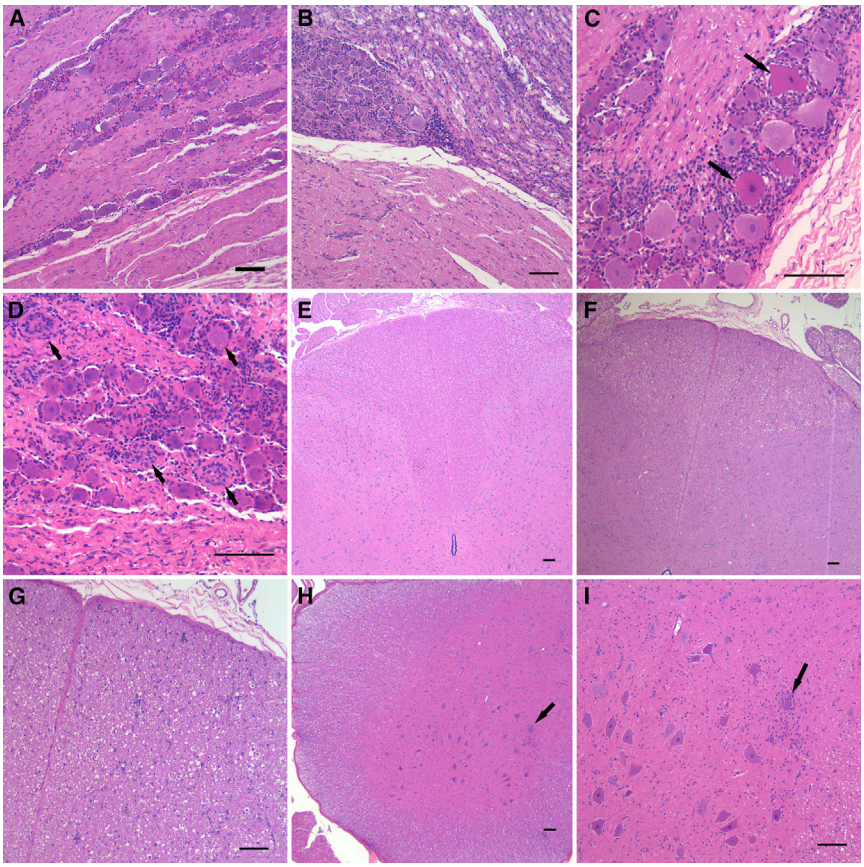

Figure 1. Representative images of test-article-related DRG and spinal cord findings

(A) Normal lumbosacral DRG in an AAV9.Null-vector-treated animal. (B) Lumbosacral DRG with increased cellularity and dorsal nerve root with degeneration and increased cellularity is shown. (C) Lumbosacral DRG with increased cellularity and degenerating neurons (arrows) is shown. (D) Lumbosacral DRG showing increased cellularity as well as glial cell hyperplasia and hypertrophy (arrows), also referred to as Nageotte nodules is shown. (E) Normal lumbar spinal cord dorsal tracts are shown. (F) Dorsal tract degeneration in the lumbar spinal cord is observed as increased clear space and cellularity. (G) Higher magnification of dorsal tract degeneration in the lumbar spinal cord is shown. (H) Gliosis in the ventral horn of the lumbar spinal cord (arrow) is shown. (I) Higher magnification of gliosis surrounding a neuron in the ventral horn of the lumbar spinal cord (arrow). The scale bars represent 100 μm in all images.

Histopathology

AAV9.hCLN2-related adverse findings were seen in the DRG, spinal nerve roots, and spinal cord from all AAV9.hCLN2-treated animals, regardless of AAV9.hCLN2 preparation method (Tables S2, S4, and S5; Figures 1 and 2), but not in the AAV9.Null-treated animals. These findings included degeneration and increased cellularity of the DRG and spinal nerve roots; they were most notable in the lumbar (L) and lumbosacral (LS) regions and in the cervical region for animals administered the highest dose (1.1×10^{14} GC/animal AAV9.hCLN2-AEX). The increased cellularity was a locally extensive to diffuse (i.e., not strictly a single focal) increase in the number of non-neuronal cells in the ganglion. The cell population was considered to be a mixture of satellite glial cells and infiltrating lymphocytes and macrophages. Neuronal degeneration was characterized by neurons that were shrunken, with hypereosinophilic (red) cytoplasm, variable vacuolation, and some infiltration by mononuclear cells (likely macrophages or lymphocytes). This change was always associated with a notable increase of cellularity around the neurons. Small foci of increased cellularity occurred commonly in the DRG of monkeys (control and treated animals). Only more diffuse infiltrates with a grade ≥ 2 (mild) were considered test article related, as less severe infiltrates were also noted in control animals. The occurrence and severity of the change varied between animals in the same group and even between ganglia at the same general region (i.e., LS) in a single animal. Although various ganglia were affected, the change tended to be most consistent in the LS ganglia. In the nerve roots, the presence of increased cellularity likely reflects the presence of macrophages as well as Schwann cell proliferation due to prior degeneration of axons and/or myelin. The degeneration in the nerve roots and sciatic nerve primarily included dilated myelin sheaths, infiltrating macrophages removing cellular debris and/or axonal and myelin fragments. In the spinal cord, the presence of axonal and/or myelin degeneration in specific white matter tracts was observed. Dorsal tracts are ascending axons, and a portion of these are axons from DRG neurons. This degeneration was interpreted to be due to test-article-related DRG neuron and/or dorsal spinal nerve root axonal damage. The presence of an increase of glial cells, in gray matter (neuronal) areas that were sometimes associated with neuronal degeneration, was noted in both the dorsal and ventral horns. In the AAV9.Null-treated animals, a higher incidence of increased cellularity (two of four animals) in the DRG (LS only) when compared with the control group (one of four animals) and degeneration in the sciatic nerve (minimal to mild) were observed but did not occur in the same animals. There were no other observations in AAV9-Null-treated animals.

In AAV9.hCLN2-treated animals only, findings in the brain included perivascular mononuclear cells in the meninges, neuronal necrosis (confirmed with Fluoro-Jade B [FJB] stain) in the cerebellum, and gliosis and microgliosis and neuronal degeneration in multiple brain levels (Tables S2 and S3).

Peripheral nerve conduction

In all animals where microscopic changes were observed in DRG, spinal nerve roots, spinal cord, and sciatic nerve, no effects were seen in

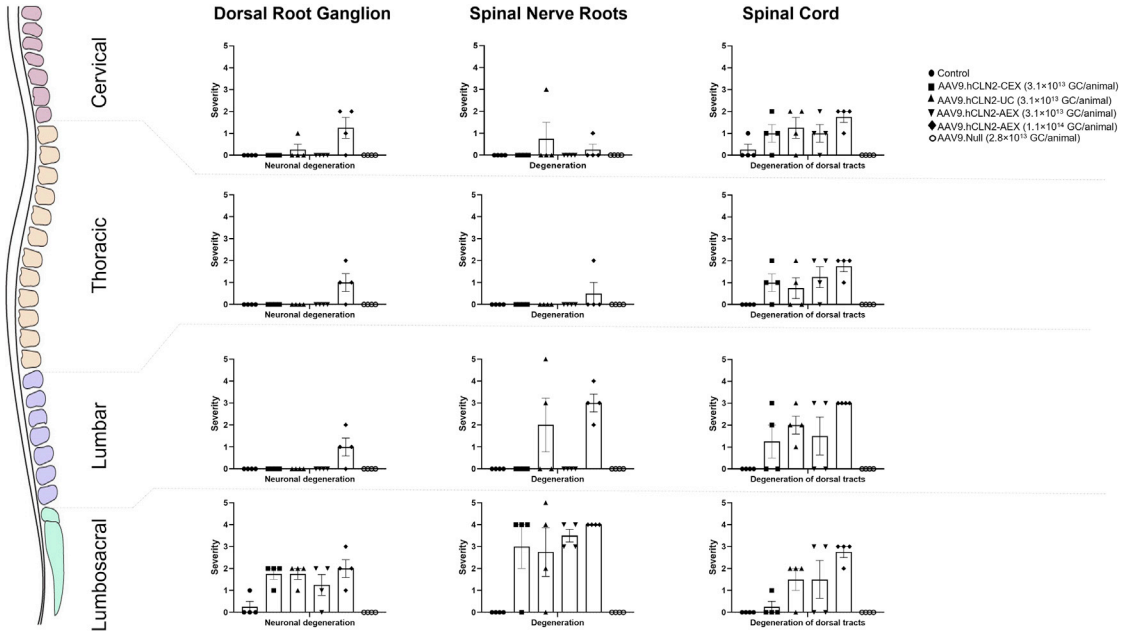

Figure 2. Summary of key changes in the DRG, spinal cord, and spinal nerve roots

Individual cumulative scores defined as the sum of cervical, thoracic, lumbar, and lumbosacral regions with 0 as not present, 1 as minimal, 2 as mild, 3 as moderate, 4 as marked, and 5 as severe. Error bars represent SEMs.

the neuro-electrophysiological endpoints (Figure 3; Tables S6–S16). This assessment focused on sensory nerve conduction testing due to the suspected DRG involvement. Nerve conduction testing can detect slowing of the conduction velocity, indicative of demyelination, and a reduction in the amplitude of sensory nerve action potentials (SNAPs) (Tables S7, S9, S11, and S13), indicative of axonopathy. In addition to sensory testing, motor nerve conduction velocity assessments using a muscle response or M-wave, F-wave (assessing ascending motor pathways), and H-reflex responses (assessing Ia fiber afferents) were also performed for one motor pathway (tibial and sciatic). All recording procedures were adapted from routinely used neurological clinical protocols.[11] No effects were detected in any of these parameters (including M-wave, F-wave, and H-reflex responses), suggesting that any functionally relevant axonopathy or demyelination in the distal portions of the nerves tested was minimal and the conduction velocity in response to stimulation remained within physiological limits. Nerve conduction can be preserved in a peripheral sensory nerve, even in the presence of minimal DRG pathology, as most peripheral sensory nerves contain axons originating in more than one DRG and neuronal degeneration does not affect DRGs uniformly. The lack of any behavioral observations or significant IENFD findings supports this conclusion.

Intraepidermal nerve fiber density

A skin biopsy was collected from the footpads to assess IENFD. Overall, when comparing the average nerve fiber density pre- and post-dose by group (Figure 4; Table S17), there was no statistically significant difference noted. However, when evaluating individual pre- and post-dose nerve fiber densities, decreases in some AAV9.hCLN2-treated animals were observed (Figure 4). Two animals (AAV9.hCLN2-CEX group; animal numbers 5 and 6) had notable reductions in nerve fiber density between the pre- and post-dose time points and were below the observed control range. These animals also had marked degeneration of the lumbosacral dorsal nerve root and moderate to marked degeneration of the sciatic nerve, histologically. Decreases below the control range in IENFD were also seen in two animals treated with AAV9.hCLN2-AEX at 3.1×10^{13} GC/animal (animal numbers 3 and 4) with degeneration of the lumbosacral dorsal root after 4 weeks, but IENFD changes were not observed at the highest dose. Thus, the reduction in nerve fiber density was considered to be likely test-article-related in some animals but showed no relationship to dose.

MRI

At 1.1×10^{14} GC/animal AAV9.hCLN2-AEX (the only AAV9.hCLN2 group evaluated), MRI findings included increased signal intensity in the spinal nerves and dorsal spinal cord on T2-weighted and STIR images, a slight decrease in fractional anisotropy in all spinal nerves and dorsal spinal cord, slight decrease in axial diffusion in most nerve pairs, slight increase in radial diffusion in all nerve pairs, and a slight decrease in radial diffusion in the spinal cord compared with pre-dose (Figures 5, 6, and 7; Tables S18–S25).

Signal intensity increased in all spinal nerves and in the dorsal spinal cord 4 weeks post-dosing compared with baseline in the AAV9.hCLN2-treated group on T2-weighted and STIR images, but

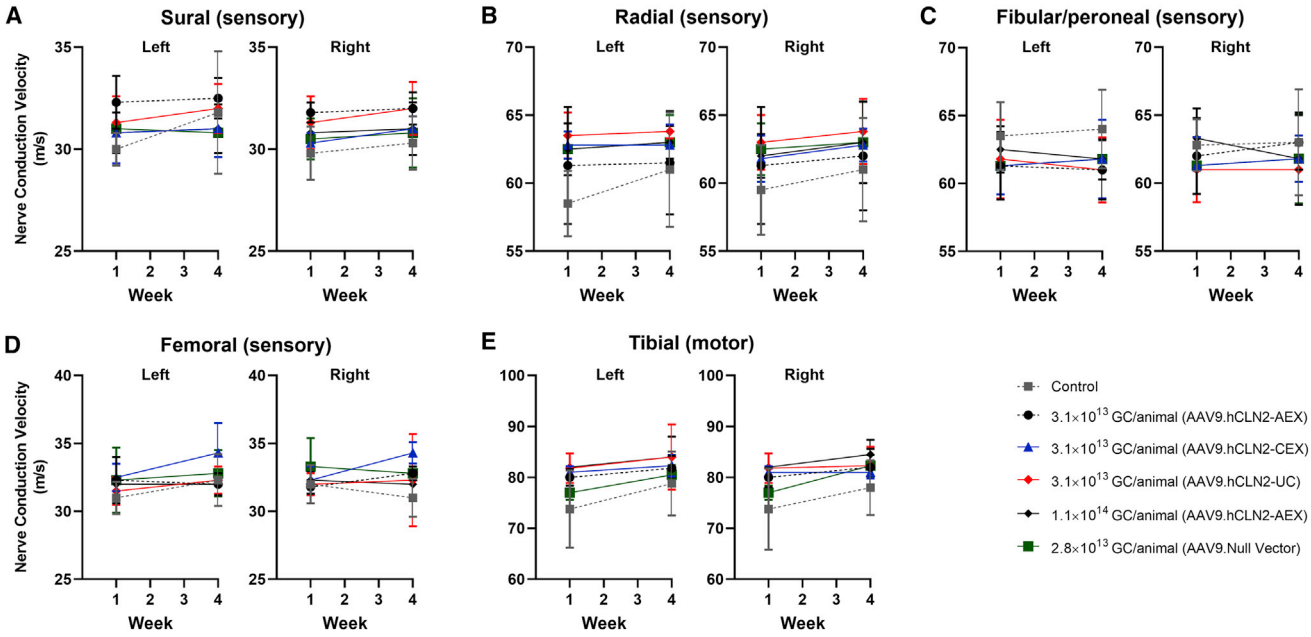

Figure 3. Summary of neuro-electrophysiological endpoints

Summary of nerve conduction velocity for (A) sural (sensory), (B) radial (sensory), (C) fibular and peroneal (sensory), (D) femoral (sensory), and (E) tibial (motor) nerves. Data were collected following direct electrical stimulation of a nerve and recording of a propagated nerve action potential at a distant location on the same nerve (sensory fibers) or the muscle innervated by the nerve (motor fibers). Mean nerve conduction velocity (m/s) is presented. Error bars represent SD.

not in control animals. The gluteal muscle signal intensity also increased on T2-weighted images in the AAV9.hCLN2 group, but not in the control animals. The gluteal muscle signal intensity did not change on the STIR images in either group, implying that the changes were likely due to fatty infiltration (e.g., secondary to denervation) and not water content (edema). The fractional anisotropy decreased in all spinal nerves and the dorsal spinal cord 4 weeks post-dosing compared with baseline in the AAV9.hCLN2 group but was not observed in control. While changes in axial diffusion varied, it decreased slightly in most nerve pairs in the AAV9.hCLN2 group. Radial diffusion increased slightly in all nerve pairs but decreased slightly in the spinal cord for the AAV9.hCLN2 group. Quantitative MRI results were compared with the histopathology data and indicated that two animals with the greatest lumbar and lumbosacral spinal cord and nerve pathology, especially with respect to spinal nerve root degeneration, exhibited the greatest decreases in lumbar spinal nerve fractional anisotropy. The animal with the least severe pathology exhibited the least change in lumbar spinal nerve anisotropy.

DISCUSSION

The aim of this study was to further elucidate the determinants of the DRG toxicity observed when rAAV vectors are administered intrathecally to NHPs. This study also included a comprehensive functional assessment of nerve conduction alongside an assessment of IENFD and imaging (MRI) at the regions of interest to characterize the impact of the histological changes and obtain measurable and translatable endpoints to use in the clinic.

We administered AAV9.hCLN2 manufactured using different purification methods and yielding varying ratios of full or empty capsids to cynomolgus monkeys and demonstrated widespread biodistribution in the brain and spinal cord alongside increases in CSF and serum TPP1 concentration (transgene expression) following a single injection into the cisterna magna. The findings described here in the spinal cord and DRG are in line with those reported for other rAAVs administered intrathecally.[4–6] We have observed that findings were similarly present using three different AAV purification methods, indicating that the purification process and relative amount of empty capsid are not major determinants of the DRG toxicity.

Alongside an assessment of the potential impact of the purification process on DRG toxicity, we assessed an AAV9.Null vector. This was designed to transduce cells as efficiently as AAV9.hCLN2 without producing mRNA from either DNA strand of the vector genome, thereby providing a control for possible toxic effects of vector transcription or encoded proteins.[12,13] When AAV9.Null was administered into the cisterna magna of cynomolgus monkeys, widespread transduction of the brain, spinal cord, and DRG was observed with vector DNA levels equivalent or greater than AAV9.hCLN2-treated animals. However, there was no evidence of DRG toxicity or any other treatment-related findings in these AAV9.Null-treated animals. This is consistent with the data reported by Hordeaux et al.,[4] who included an miR183 target in their construct in order to reduce the abundance of the transgene mRNA in DRG neurons. Interestingly, when AAVrh10.hARSA or AAVrh10.Null vector was administered

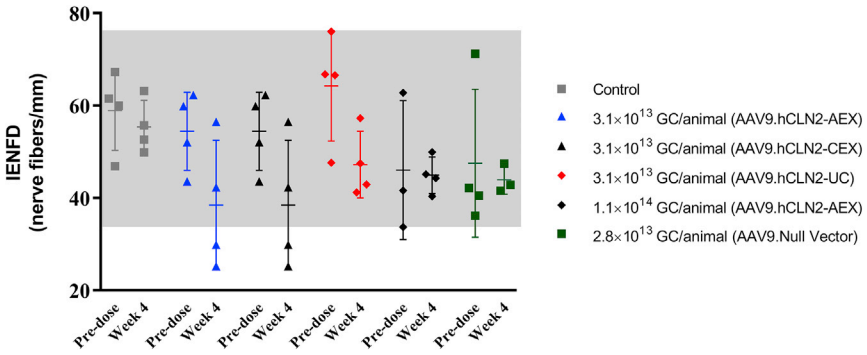

Figure 4. Summary of intra-epidermal nerve fiber density (IENFD)

Skin biopsies were collected prior to treatment and at necropsy, sectioned, and stained using Protein Gene Product 9.5. Axons were counted as they crossed the dermal/epidermal junction, and the number of axons per linear millimeter of epidermal/dermal junction was calculated. Bars represent mean and SD; the gray shaded area represents the range of pretreatment values from samples collected.

to NHPs via intraparenchymal injection, axonal degeneration was observed in the spinal cord in both groups of animals.[14] The AAVrh10.Null vector used in that study had a functional CAG promoter (same promoter as used with AAV9.hCLN2, referred to as CB7), but no translatable protein product; therefore, it will produce a high level of mRNA but no protein. This is different than the AAV9.Null vector used in our study, which lacked a functional promoter and does not produce mRNA or protein. Therefore, the data from this study suggest that the findings observed in the DRGs of NHPs may be an overexpression-related injury and corroborate the data generated by Hordeaux et al.[4] That the lumbar and lumbosacral region is particularly sensitive may be due to the high biodistribution and transgene expression at this level or may reflect that the metabolic stress on these DRGs with their long ascending and descending neurons leads to subsequent axonal degeneration.

In AAV9.hCLN2-treated animals only, findings in the brain were unique to this transgene and not described in NHPs for either AAV9.CB7.hIDUA or AAV9.CB7.hIDS that have the same vector and promoter. Furthermore, these were not seen in the brain of animals administered the AAV9.Null vector.[5,6] Therefore, the findings in the brain were possibly an immune-mediated response to the human TPP1 (TPP1 amino acid sequence homology for monkey compared with human is 98%), as most animals elicited a humoral response to the human transgene product and similar findings attributed to transgene product immunogenicity have been described previously.[15]

As well as elucidating the mechanism of action for these changes, it is also important to understand the relevance of these findings from a functional perspective and, more importantly, how to monitor such findings in clinical studies. In the nonclinical studies conducted with AAV9.hCLN2 as well as AAV9.CB7.hIDUA and AAV9.CB7.hIDS, there have been no clinical signs associated to the histological changes.[5,6] Therefore, as these findings were asymptomatic, a more sensitive measurement of functionality was performed by neuro-electrophysiological assessment (nerve conduction). At 4 weeks, when the DRG toxicity was observed, there were no abnormalities detected following a thorough evaluation of nerve conduction (sensory and motor), F-wave (testing ascending motor pathways), and the H-reflex (or Hoffmann's reflex). This suggests that, functionally, the nerves remained within the normal limits of conduction despite the histological changes observed, indicating that sufficient fibers remained intact to respond to stimulation. A low incidence of functional correlates aligns with published meta-analysis where minimal-to-moderate pathology was not associated with clinical symptoms and more severe pathology was associated with changes in nerve conduction in only 2 of 56 animals at 28 days post-intrathecal injection of AAVs.[4] In the current study, no functional electrophysiological abnormalities were detected in the 16 animals administered AAV9.hCLN2 in the presence of DRG changes.

Electrophysiological tests of nerve conduction are translatable across species and the gold standard differential diagnostic test of disease in the neurology clinic. Neuro-electrophysiological correlates of drug-induced toxicity have been established for multiple classes of compounds, and the technique is well established in the preclinical space.[16] Some limitations need to be taken into account, however, when interpreting mild toxicity based on nerve conduction. Electrophysiological assessments are capturing nerve impulse conduction across relatively fast fibers, which underlie the majority of a sensory nerve's normal function. The distribution of velocities in a nerve is reflected by the action potential morphology, which is quantitatively captured by nerve conduction measurements. The contribution of each axon to the compound action potential recorded with nerve conduction techniques depends both on its size and the degree of myelination. Axons are myelinated to various degrees in any nerve, ranging from 1 to 20 μm in diameter for fast myelinated fibers and from 0.2 to 3 μm in unmyelinated ones.[17] If only a small subset of large axons is affected or if the neuropathy affects only very small unmyelinated fibers, the conduction velocity of the whole nerve can remain normal, lacking clinical abnormalities. Behavioral observations indicative of pain in the extremities, such as gait changes, may point to small fiber neuropathies not captured by nerve conduction. Further, normal nerve conduction can be preserved in a peripheral sensory nerve in the presence of limited DRG pathology, as peripheral sensory nerves contain axons originating in more than one DRG and neuronal degeneration does not affect DRGs uniformly. Therefore, in the case of mild toxicity, a weight of evidence approach is useful, including clinical observations, MRI, and epidermal fiber assessment.

In addition to an assessment of neuro-electrophysiological parameters, samples of skin were collected from the footpad of cynomolgus

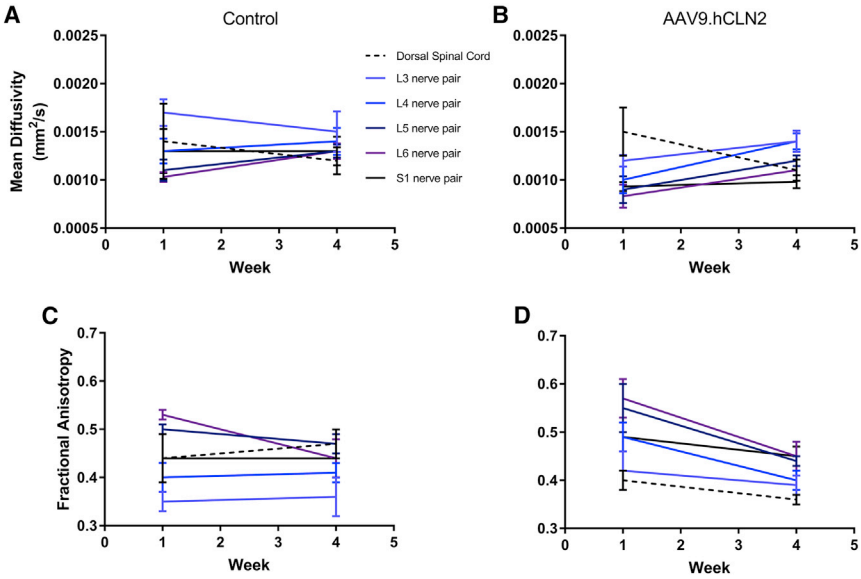

Figure 5. Mean diffusivity and fractional anisotropy at baseline and 4 weeks post-dosing

MR images were acquired from (A) control and (B) AAV9.hCLN2-AEX (1.1×10^{14} GC/animal) or fractional anisotropy from (C) control and (D) AAV9.hCLN2-AEX (1.1×10^{14} GC/animal) at two time points: baseline (before dosing, labeled as week 1) and 4 weeks post-dosing with a 3 T Phillips Achieva MRI scanner with Flex L and spine radiofrequency (RF) coils. Pulse sequences were qualitatively reviewed by a board-certified veterinary radiologist and appropriate sequences selected based on spatial resolution and image contrast for region of interest (ROI) creation and signal intensity measurement. Images selected include DTI high iso for mean diffusivity. Statistical analyses were performed, comparing groups against their baseline (Tables S18–S25). A $p < 0.05$ was seen for mean diffusivity at L6 in AAV9.hCLN2-treated animals.

monkeys administered AAV9.hCLN2 for an assessment of IENFD, an endpoint that can be used to assess peripheral neuropathy. The number of nerve fibers are determined by counting nerve fibers crossing the dermal/epidermal junction and, with peripheral neuropathy, can confirm small unmyelinated nerve fiber damage as seen in HIV-related sensory neuropathy.[18] In cynomolgus monkeys administered AAV9.hCLN2, there was no consistent decrease in IENFD observed after 4 weeks, with the exception of a few animals. In two animals, the decrease in IENFD correlated with a greater severity of axonal degeneration observed. However, these decreases did not correlate with any functional effects seen in neurography. It is unclear whether or not these changes would have been more apparent in a study of a longer duration.

MRI was evaluated using a 3T Philips scanner (acquired with the Flex L and Spine coils) from regions of interest within the spinal cord (L1–S3) that correlate to where the changes primarily occur. This was performed in control and AAV9.hCLN2-treated animals at the highest dose tested (1.1×10^{14} GC/animal) prior to dosing and after 4 weeks. In animals observed with axonal degeneration, MRI findings included increased signal intensity in the spinal nerves and dorsal spinal cord on T2-weighted and STIR images, a slight decrease in fractional anisotropy in all spinal nerves and dorsal spinal cord, slight decrease in axial diffusion in most nerve pairs, slight increase in radial diffusion in all nerve pairs, and slight decrease in spinal cord. Furthermore, quantification of the MRI changes exhibited the greatest decreases in lumbar spinal nerve fractional anisotropy in animals with a greater severity of spinal nerve root degeneration. The two subjects with the greatest pathology each had two or more spinal nerve pairs with at least 24% reduction in fractional anisotropy. Similar magnitude reduction of fractional anisotropy was observed associated with clinical deficits in a feline model of demyelination and in human patients with entrapped lumbar nerves.[19,20] Reductions in fractional anisotropy of white matter are attributed to demyelination, gliosis, or disruption of axonal alignment and have been reported associated with multiple sclerosis, amyotrophic lateral sclerosis (ALS), and Alzheimer's disease among other disorders.[19,21] In this study, an increase in T2-weighted signal intensity was also observed in gluteal muscle of animals administered AAV9.hCLN2, but not observed in STIR images of gluteal muscle, suggesting that the intensity changes were due to fatty infiltration (e.g., secondary to denervation) and not edema. Fatty infiltration of muscle has been observed via MRI associated with a number of underlying neuropathologies, including traumatic nerve injury, muscular dystrophy, ALS, cerebral palsy, and poliomyelitis.[22–24] Therefore, it may be possible to use MRI around the regions of interest where the histological changes were observed to correlate these findings with a clinically available endpoint. The DRG toxicity seen with AAV9.hCLN2, as well as AAV9.CB7.hIDUA and AAV9.CB7.hIDS, do not appear to correlate with changes described in one ALS patient administered AAVrh10, which appeared more immune mediated.[5,6,25] In this study, one patient was described with peripheral neuropathy and, alongside elevations in alanine aminotransferase (ALT) and T cell response to viral capsid, severe decreases in sural SNAP, left median sensory potential, and H-reflexes and contrast enhancement of the DRG and spinal nerves at L3–L4 and L4–L5, indicative of active inflammation.[25] In studies with AAV9 in NHPs, changes in interferon γ (IFNγ) (enzyme-linked immunosorbent spot [ELISPOT]) to either the transgene product or capsid were observed but did not correlate with DRG pathology; immune suppression ablated T cell responses, but not DRG pathology; and nerve conduction was within normal limits for all animals.[5,6] To date, clinical findings associated with dorsal root ganglionopathy have not been described for AAV9s, including onasemnogene abeparvovec and AAV9.CB7.hIDS following administration of AAV9 to humans in multiple clinical trials.[26–28]

In conclusion, when cynomolgus monkeys were administered AAV9.hCLN2 into the cisterna magna, neuronal degeneration,

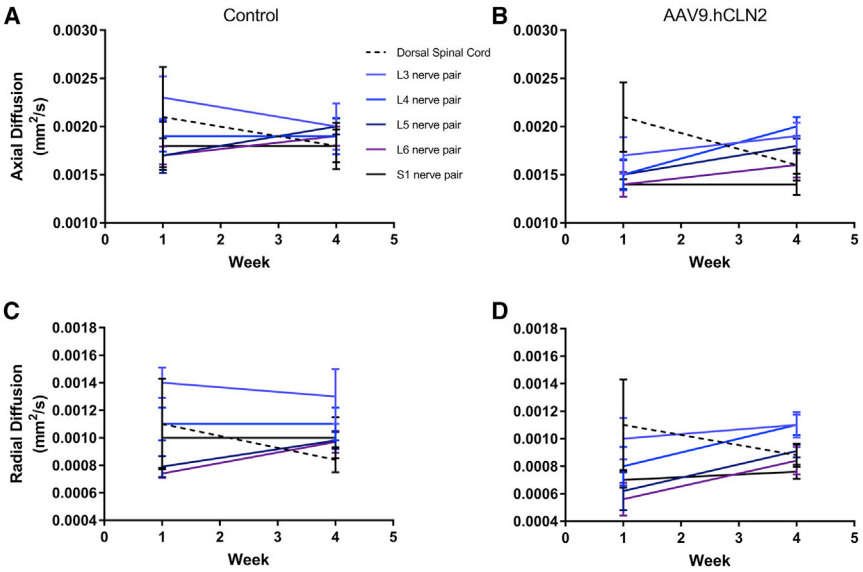

Figure 6. Axial and radial diffusivity at baseline and 4 weeks post-dosing

MR images were acquired for axial diffusion from (A) control and (B) AAV9.hCLN2-AEX (1.1×10^{14} GC/animal) or radial diffusion from (C) control and (D) AAV9.hCLN2-AEX (1.1×10^{14} GC/animal) at two time points: baseline (before dosing, labeled as week 1) and 4 weeks post-dosing with a 3 T Phillips Achieva MRI scanner with Flex L and spine RF coils. Pulse sequences were qualitatively reviewed by a board-certified veterinary radiologist and appropriate sequences selected based on spatial resolution and image contrast for ROI creation and signal intensity measurement. Images selected include DTI high iso for axial and radial diffusivity. Statistical analyses were performed, comparing groups against their baseline (Tables S18–S25). A $p < 0.05$ was seen for axial diffusivity at L6 in AAV9.hCLN2-treated animals.

primarily lumbar and lumbosacral regions, with increased cellularity that is associated with secondary degeneration of ascending sensory nerve fibers and descending fibers from peripheral nerves (sciatic nerve), was observed. These changes were not associated with differences in the purification process and subsequent differences in empty/full capsid ratio. They were also not observed with an AAV9.Null vector that does not produce mRNA. Therefore, this study alongside other published data supports a hypothesis that the DRG toxicity in NHPs following intrathecal administration of rAAV9 is primarily mediated by transgene overexpression. That these findings do not correlate with any clinical observations or notable effects on nerve conduction indicates that these changes are sub-clinical, and long-term studies in NHP suggest they resolve over time.[10] That the DRG changes were detectable using MRI also opens up the possibility to include this assessment as an exploratory endpoint in clinical studies with AAV9s alongside careful monitoring and supporting data from clinical studies.

MATERIALS AND METHODS

Animals

All animal procedures were approved by Northern Biomedical Research (NBR) IACUC, and all experiments conform to all relevant regulatory standards. Cynomolgus monkeys that screened negative for anti-AAV9 NAbs were purchased from Alpha Genesis (Yemassee, SC). Animals were housed in an AAALAC-accredited facility in compliance with National Institutes of Health (NIH) guidelines and the Animal Welfare Act on a 12:12 h light:dark cycle. They were fed monkey biscuits (PMI Certified Primate Diet no. 5048; 20 biscuits/day) and filtered municipal water *ad libitum*.

Study design

Groups of cynomolgus monkeys (2/sex/group) were administered a single dose of vehicle, Null AAV9 vector (referred to as AAV9.Null), or different preparations or doses of AAV9.CB7.hCLN2 (referred to as AAV9.hCLN2; Table 1) via cisterna magna puncture (1 mL/animal). At the end of the study (day 30), animals were euthanized following sedation (8 mg/kg ketamine HCl intramuscularly [i.m.]) and perfused via the left cardiac ventricle with 0.001% sodium nitrite in saline under anesthesia. Endpoints included clinical observations, body weight, food consumption (qualitative), pharmacodynamics (TPP1 concentration [serum and CSF]), immunogenicity (anti-TPP1 antibodies and anti-AAV9 NAbs), biodistribution, organ weights, and macroscopic and microscopic examination. At the time of necropsy, the brain was cut in a brain matrix at 3-mm coronal slice thickness and sections collected for histology, TPP1 concentration, and biodistribution. For TPP1 concentration and biodistribution, 4-mm-round samples of frontal cortex, occipital cortex, cerebellum, striatum, medulla oblongata, midbrain, and thalamus were placed in labeled vials, snap frozen on dry ice, and stored at −60°C or below. One sample from each area was superficial (<3 mm deep), and the other sample from each area was deep (>3 mm deep). At necropsy, the spinal cord with attached spinal nerve roots and ganglia was divided into cervical, thoracic, and lumbar and sacral sections. A 1-cm segment from each section was collected for TPP1 concentration and biodistribution. Any associated spinal nerve root or ganglia from the biodistribution section was removed and frozen separately (in left and right pairs). The remaining portion of the spinal cord was fixed in 10% neutral buffered formalin (NBF) for histological analysis. Samples were also collected from the kidneys, ovaries, sural nerve, eyes (with optic nerve), liver (with gallbladder), sciatic nerve, testes (with epididymides), lungs (with bronchi), tibial nerves, heart, lymph nodes, and trigeminal ganglia.

Test article

The test articles used in this study consist of the rAAV9 containing either a vector genome encoding the human lysosomal enzyme TPP1, AAV9.CB7.hCLN2, or a vector genome that does not produce mRNA or protein, AAV9.Null. In AAV9.CB7.hCLN2, the TPP1 transgene sequence is flanked by AAV2 inverted terminal repeats

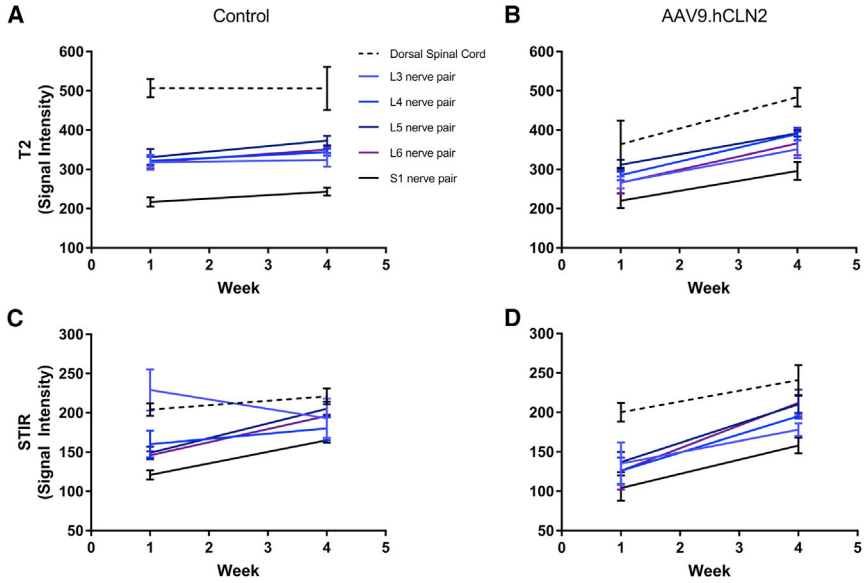

Figure 7. s2 neuro T2-TFE signal intensity and STIR signal intensity at baseline and 4 weeks post-dosing

MR images were acquired for s2 neuro T2-turbo field echo (TFE) from (A) control and (B) AAV9.hCLN2-AEX (1.1×10^{14} GC/animal) or 3D STIR from (C) control and (D) AAV9.hCLN2-AEX (1.1×10^{14} GC/animal) at two time points: baseline (before dosing, labeled as week 1) and 4 weeks post-dosing with a 3 T Phillips Achieva MRI scanner with Flex L and spine RF coils. Pulse sequences were qualitatively reviewed by a board-certified veterinary radiologist and appropriate sequences selected based on spatial resolution and image contrast for ROI creation and for assessment of s2 neuro T2-TFE or 3D STIR images. Statistical analyses were performed comparing groups against their baseline (Tables S18–S25). A $p < 0.05$ was seen for s2 neuro T2-TFE signal intensity at L6 and STIR signal intensity at L3, L4, L5, L6, and S1 in AAV9.hCLN2-treated animals.

(ITRs) and its expression is driven by a CB7 promoter, a hybrid between a cytomegalovirus (CMV) immediate-early enhancer and the chicken β-actin promoter. Transcription from this promoter is enhanced by the presence of the chicken β-actin intron (CI). The polyadenylation signal for the expression cassette is from the rabbit β-globin (RBG) gene.

The purification processes utilized for the AAV9 vector preparations used in this study have been described previously and include a standard AEX or processes that used as an additional step prior to the AEX either CEX or an UC.[29,30] The resulting vectors are referred to as AAV9.hCLN2-AEX, AAV9.hCLN2-CEX, and AAV9.hCLN2-UC. AAV9.Null was purified by the AEX process.

In AAV9.Null, the genome sequence contains 5′ ITR, RBG polyA, CpG-depleted CI, human RPE65 cDNA with start codon mutated and reading frame disrupted, and 3′ ITR. RBG polyA allows accurate droplet digital PCR (ddPCR) titer comparison with other AAV9s and eliminates any potential transcription from ITR. To confirm that the Null vector did not produce transgene RNA, human iCell GlutaNeurons were transduced at a multiplicity of infection (MOI) of 3×10^5 GC/cell with either an AAV9 vector expressing a synthetic microRNA (miRNA) (AAV9.miR) or AAV9.null (n = 4 wells for each condition). Cells were harvested 9 days after transduction, total RNA was isolated, and libraries prepared and sequenced using the Illumina HiSeq platform. Following read mapping to the human_hg38 reference genome and normalization, read counts for genes of interest were obtained. As anticipated, no reads mapping to human RPE65 (ENSG00000116745) were detected in samples treated with AAV9.miR, as RPE65 expression is not expected in glutamatergic neuronal populations. In samples treated with AAV9.null, an average of 25 reads mapping to human RPE65 was detected per sample. While detectable, this level of RPE65 expression can be considered negligible, as these reads comprised, on average, less than 0.00018% of all normalized reads, many orders of magnitude lower than the expression level of a number of commonly used housekeeping genes. This expression level is also significantly lower than what we would expect to see from a standard AAV expression cassette following *in vitro* transduction of a construct containing the proper promoter, polyA, and start codon elements in the proper orientation. Therefore, the modifications made to the AAV9.null expression cassette were shown to attenuate production of transgene RNA.

Dose administration

Animals received vehicle or one of the test articles via an intrathecal cisterna magna (CM) puncture injection under anesthesia. Each animal was provided dexmedetomidine hydrochloride (0.04 mg/kg, i.m.) followed by ketamine hydrochloride (2.5 mg/kg; i.m.). Once sedated, the animals were intubated and placed in a lateral recumbent position, and the spinal tap was performed with a Gertie Marx introducer and 22G needle. The introducer (gauge not provided by manufacturer) remained in place throughout CSF collection and dose administration to support the placement of the spinal needle in the CM. Access to the CM was confirmed by the flow of CSF from the needle. Once CSF was observed in the hub of the spinal needle, a collection vial was placed below the needle and CSF collected. Following CSF collection, the 1 mL dose was administered over approximately 1 min by manual bolus followed by 0.25 mL vehicle flush by manual bolus. The spinal needle remained in the CM for approximately 30 s after the completion of the dose. Once the needle and introducer were removed, direct pressure was applied to the injection site followed by application of a topical aseptic ointment. The reversal agent, atipamezole hydrochloride (0.2 mg/kg; i.m.), was administered and the animal returned to its cage.

In-life parameters

Animals were checked frequently and clinical signs recorded twice daily. Body weights were recorded for all animals prior to dose

administration for randomization, on the day of dose administration, weekly during the study, and at necropsy. Food consumption was monitored visually by qualitative assessment.

Assessment of transgene product (TPP1 concentration) in serum and CSF

Samples of blood were collected on days 1 (prior to dosing), 4, 8, 15, and 22 and prior to necropsy for serum TPP1 concentration. CSF was collected on days 1 (prior to dosing) and 15 and prior to necropsy for TPP1 concentration. TPP1 concentration was determined by an electrochemiluminescent (ECL) immunoassay implemented using the Meso Scale Discovery (MSD) platform. Briefly, biotinylated monoclonal anti-TPP1 antibody (R&D Systems no. MAB2237) was added to a streptavidin-coated MSD plate that has been blocked before use. After incubation, unbound antibody was washed from the plate followed by addition of samples, including calibration standards, quality controls (QCs), and study samples. After incubation, the plate was washed and any TPP1 protein captured by the immobilized antibody was detected by a polyclonal anti-TPP1 antibody (R&D Systems no. AF2237) labeled with SULFO-TAG. Following a wash step, the bound SULFO-TAG-labeled anti-TPP1 was detected with tripropylamine containing MSD read buffer. The intensity of the chemiluminescent signal, which was directly proportional to the amount of TPP1 present in the sample, was measured in an MSD reader. Calibration standard curves were prepared using the recombinant human TPP1 ranging from 0.0205 to 12.0 ng/mL. Concentrations of TPP1 in the study samples were determined by comparing the chemiluminescent signals to that of the standard curves. This assay was characterized following the principles described in the Bioanalytical Method Validation Guidance document (Food and Drug Administration, 2018). Results of the qualification experiments demonstrated that the performance of the assay was accurate, precise, and specific in monkey matrices within the determined range of the assay and was suitable for study sample analysis.

Immunogenicity

Immunogenicity, as either anti-TPP1 antibodies or anti-AAV9 NAbs, was analyzed from samples of blood collected prior to dosing (week −1) and prior to necropsy. All assays were characterized following the principles described in the Immunogenicity Testing of Therapeutic Protein Products - Developing and Validating Assays for Anti-Drug Antibody Detection (Food and Drug Administration, 2019).

The detection of anti-TPP1 antibodies used a solution-bridging ECL immunoassay implemented using the MSD platform. Samples, including negative and positive controls and study samples, were acidified by incubating with 300 mM acetic acid. The acidified samples were neutralized with 1M Tris base solution in the presence of a reaction mixture containing biotinylated recombinant human TPP1 (TPP1-Biotin) and SULFO-TAG-labeled recombinant human TPP1 (TPP1-ST). Anti-TPP1 antibodies in samples bound to the labeled TPP1 forming bridging complexes containing TPP1-Biotin and TPP1-ST. After incubation, the mixtures were added to a streptavidin-coated MSD plate that had been blocked before use, and the TPP1-Biotin was captured by the streptavidin in the wells. The plate was then washed and a tripropylamine containing MSD read buffer was added to the plate to produce a chemiluminescent signal in proportion to the amount of anti-TPP1 antibodies in the samples. Samples were screened for reactivity and considered reactive if their mean response values were greater than the plate screening cut point. The screened positive samples were semi-quantified by serially diluting samples in a negative control matrix to lower the detection signal below the assay cut point. The titer was determined as the reciprocal of the highest serial dilution yielding a response greater than the assay cut point. Assay cut points for antibody screening and titration were determined prior to sample analysis. The methods were successfully qualified, and the results of the qualification experiments demonstrated that the performance of the assay was consistent with the targeted acceptance specifications in terms of system suitability, cut point determination, precision, sensitivity, selectivity, specificity, drug tolerance, and analyte stability in monkey serum.

For anti-AAV9 NAbs, a cell-based transduction efficiency assay was used to detect the presence of anti-AAV9 NAbs in cynomolgus monkey serum, by measuring the inhibition of the transduction of an AAV9-luciferase reporter vector in 293T cells. The method detects the presence of both pre-existing or treatment-induced NAbs to AAV9. In brief, 96-well plates were seeded with cultured 293T cells and incubated overnight at 37°C and 5% CO2. Serum samples, including negative control, positive control, and study samples, were mixed 1:1 with AAV9-Luciferase vector in DMEM with 1% BSA for 1 h at 37°C before addition to cells in duplicate wells. On the following day, media were removed and cells were lysed in buffer containing the Steady-Glo luciferase substrate (Promega Cat no. E2510). Luminescence was measured on a PerkinElmer Envision plate reader. The NAb titer was reported as the reciprocal of the highest serum dilution that inhibited AAV transduction by 50% compared with the negative control (100% transduction). The results of development experiments demonstrated that the performance of the assay was consistent with the targeted specifications in terms of preparation of negative controls, selection of positive controls, MOI determination, assay sensitivity, and assay system suitability.

Nerve conduction assessment

Neuro-electrophysiological evaluations of peripheral nerve function were performed in all animals prior to dosing and at the end of week 4. All recording procedures were adapted for primates from routinely used neurological clinical protocols.[11] Briefly, nerve conduction assessment involves direct electrical stimulation of a nerve and recording of a propagated nerve action potential at a distant location on the same nerve (sensory fibers) or the muscle innervated by the nerve (motor fibers), allowing an accurate localization of focal lesions or the detection demyelination or axonopathies across the portion of the nerve investigated.

All signal collections and post-collection data analyses were performed with a Natus Neurology System with Synergy software. Subdermal sterile platinum needle electrodes, less than 12 mm/0.3 mm,

or equivalent were used for recording. A pediatric stimulator was used for eliciting all evoked potentials. Signal analyses were performed post-collection to generate the sensory and motor nerve conduction velocity (NCV), SNAP amplitude, and compound muscle action potential (CMAP) amplitude and to identify the presence of the F-wave and the H-reflex.

Motor nerve function was assessed by eliciting CMAPs from a distal flexor muscle innervated by the nerve, following orthodromic stimulation of the nerve at two locations along its course. SNAPs were elicited in sensory nerves with antidromic depolarizing stimulation, with recording electrodes positioned directly over the nerve. The stimulus strength was progressively increased until a supramaximal response was evoked. Approximately 10 supramaximal stimuli were averaged for each sensory nerve.

Sensory nerve conduction was assessed in four nerves, bilaterally, in order to sample conduction velocity in branches stemming from the lumbosacral or cervical plexus (sural, S1/S2; deep fibular and peroneal, L5; medial femoral cutaneous, L2/L3; radial, C6). Motor nerve conduction was assessed bilaterally for the entire tibial motor nerve and included bilateral F-wave tests for ascending motor pathways. H-reflexes were assessed bilaterally at the soleus muscle. F-waves and H-reflexes were noted as present or absent.

Each animal was provided dexmedetomidine hydrochloride (0.04 mg/kg; i.m.) followed by ketamine hydrochloride (2.5 mg/kg; i.m.) to induce sedation, and these were not expected to affect the neuro-electrophysiological endpoints evaluated. The animal was placed on a temperature-controlled warming pad to maintain constant physiological body temperature. Following evaluation, the reversal agent atipamezole hydrochloride (0.2 mg/kg; i.m.) was administered.

Magnetic resonance imaging (MRI)

MRI scans were performed on animals from two groups only, vehicle (group 1) and high-dose AAV9.hCLN2-AEX-treated (group 5) animals prior to dosing and in week 4. Animals were pretreated with atropine sulfate (0.04 mg/kg; subcutaneously [s.c.]) followed by ketamine hydrochloride (8 mg/kg; i.m.) to induce sedation. The animals were intubated and maintained on approximately 1 L/min of oxygen and 1%–3% isoflurane as required.

MRI scans were acquired with a 3 tesla (T) Philips Achieva MRI scanner with Flex L and spine radiofrequency (RF) coils around the region of interest (ROI) from L3 to S1 and included gluteal muscle (Figure S10). Images selected included diffusion tensor imaging (DTI) high iso (to generate fractional anisotropy [FA], mean diffusivity [MD], axial diffusivity [AD], and radial diffusivity [RD]), STIR, and T2-weighted s2 neuro T2-turbo field echo (TFE). Mean signal intensity within each ROI for TFE, STIR, and diffusion maps were extracted and exported to a spreadsheet via Vivoquant with Python software for data analysis.

Skin biopsy

A skin biopsy from all animals was collected from the footpads to assess IENFD prior to dose administration and at necropsy. Skin biopsies were obtained from the plantar aspect of the foot (bilateral) while the animal was under anesthesia. The location of the biopsy was collected beneath the second digit of the right and left hind limbs during the prestudy interval and collected beneath the fourth digit of the right and left hind limbs at the necropsy interval. The biopsies were placed in a single cassette (right and left identification maintained) in chilled Zamboni's fixative and stored refrigerated for approximately 12–16 h; multiple cassettes were placed in a single container of fixative. Following fixation, the Zamboni's fixative was discarded and the samples were rinsed (three times) with sufficient 0.1M Sorensen's buffer to easily cover the cassettes. Following the final rinse, the 0.1M Sorensen's buffer was discarded and the container was filled with cryoprotectant solution (20% glycerol/0.08 M Sorensen's buffer).

The skin biopsies were sectioned using a sliding and freezing microtome set for a 50-μm advance. Sections (randomly selected) were stained, free floating, using Protein Gene Product 9.5 (PGP 9.5) to detect axons. All stained sections were mounted to glass slides. Up to three of the sections were used for the quantitative investigation. Briefly, axons were counted as they cross the dermal/epidermal junction. The length of the dermal/epidermal junction was measured. The number of axons per linear millimeter of epidermal/dermal junction was calculated. This quantitative investigation was performed with the pathologist blinded to the treatment status of the animal. All slides were coded prior to counting.

Biodistribution

Samples of brain, spinal cord and DRG (cervical, thoracic, and lumbar), proximal sciatic nerve, lymph node (inguinal, mandibular, and mesenteric), heart, kidney, liver, lung, ovary, eye (retinal choroid and sclera), and testes were collected for biodistribution. Biodistribution was assessed by real-time quantitative polymerase chain reaction (qPCR) for detection of AAV9.hCLN2 or AAV9.Null vector DNA (forward primer: 5′-TTCCCTCTGCCAAAAATTATGG-3′; reverse primer: 5′-CCTTTATTAGCCAGAAGTCAGATGCT-3′; probe: 5′ – 6FAM – ACA TCA TGA AGC CCC – MGBNFQ – 3′). The resulting copy numbers per microgram DNA for each tissue were calculated based on standard calibration curve included in each plate with control plasmid DNA. The results are normalized to one microgram of DNA, with results less than 50 copies/μg DNA (the lower limit of quantitation [LLOQ]) reported as below the limit of quantitation (BLQ). The upper limit of quantification was 5×10^8 vector copies/μg DNA. Inter- and intra-assay precision and accuracy assessments fulfilled the assay criteria for all concentrations tested.

Histopathology

At necropsy, samples of tissues were collected, and the following tissues were examined microscopically: brain regions including neocortex (including frontal, parietal, temporal, and occipital cortex); paleocortex (olfactory bulbs and/or piriform lobe); basal nuclei

(including caudate and putamen); limbic system (including hippocampus and cingulate gyri); thalamus and hypothalamus; midbrain regions (including substantia nigra); cerebellum; pons region; and medulla oblongata. Sections were embedded in paraffin, sectioned at 5 μm, stained with hematoxylin and eosin (H&E), and examined microscopically. In addition, selected sections from the brains from all animals were stained with Fluoro-Jade B (FJB) and immunohistochemically labeled ionic calcium binding adaptor molecule 1 (IBA-1) (concentrating on caudal sections) and glial fibrillary acidic protein (GFAP) (concentrating on caudal sections) and examined. At least four levels of the spinal cord from all animals (cervical, thoracic, lumbar, and lumbosacral) were embedded in paraffin, sectioned using a 5-μm block advance, and stained with H&E. Spinal nerve roots and ganglion (taken at mid-cervical, mid-thoracic, mid-lumbar, and lumbosacral) were embedded in paraffin, sectioned using a 5-μm block advance, and stained with H&E. For the sciatic nerve, a longitudinal section of the sciatic nerve was embedded in paraffin, sectioned using a 5-μm block advance, and stained with H&E.

Statistical analysis

Statistical analyses were performed on IENFD, nerve conduction, and MRI data; however, due to the small sample size in each group (n = 2 per sex/group), there may not be adequate power to identify biologically relevant differences as being statistically significant. Statistical analyses (differences from baseline within each group) were conducted using a two tailed Student's t test ($p \leq 0.05$ was considered statistically significant).

SUPPLEMENTAL INFORMATION

Supplemental information can be found online at https://doi.org/10.1016/j.omtm.2022.01.013.

ACKNOWLEDGMENTS

This study was sponsored by REGENXBIO Inc. We would like to thank all the technical staff at Northern Biomedical Research for assistance with handling, care, MRIs, sample collection, surgical, and euthanasia procedures during the *in vivo* study. We would like to thank Lovelace for the generation of biodistribution data. We would also like to thank Vector Core, Technical Operations REGENXBIO for the generation and supply of the AAVs used in this study.

AUTHOR CONTRIBUTIONS

N.B. performed conceptualization, formal analysis, investigation, methodology, project administration, supervision, and writing – original draft. L.L., M.B., J.Z., E.A., D.C., M.M., M.H., L.Y., E.B., K.H.K., and Y.L. performed investigation, methodology, project administration, resources, and writing –review & editing. M.F. and O.D. performed conceptualization and writing – review & editing.

DECLARATION OF INTERESTS

N.B., M.H., K.H.K., E.B., L.Y., Y.L., O.D., and M.F. are currently employees of REGENXBIO Inc. L.L. was an employee of StageBio at the time of study and is currently an employee of Charles River Laboratories; D.C. is currently an employee of Invicro, A Konica Minolta Company; M.M. is an employee of Preclinical Electrophysiology Consulting, LLC; J.Z. and E.A. were employees of Northern Biomedical Research at the time of study; and M.B. is an employee of StageBio.

REFERENCES

1. Kuzmin, D.A., Shutova, M.V., Johnston, N.R., Smith, O.P., Fedorin, V.V., Kukushkin, Y.S., van der Loo, J.C.M., and Johnstone, E.C. (2021). The clinical landscape for AAV gene therapies. Nat. Rev. Drug Discov. *20*, 173–174.

2. Mendell, J.R., Al-Zaidy, S.A., Rodino-Klapac, L.R., Goodspeed, K., Gray, S.J., Kay, C.N., Boye, S.L., Boye, S.E., George, L.A., Salabarria, S., et al. (2021). Current clinical applications of in vivo gene therapy with AAVs. Mol. Ther. *29*, 464–488.

3. Bolt, M.W., Brady, J.T., Whiteley, L.O., and Khan, K.N. (2021). Development challenges associated with rAAV-based gene therapies. J. Toxicol. Sci. *46*, 57–68.

4. Hordeaux, J., Buza, E.L., Dyer, C., Goode, T., Mitchell, T.W., Richman, L., Denton, N., Hinderer, C., Katz, N., Schmid, R., et al. (2020). Adeno-associated virus-induced dorsal root ganglion pathology. Hum. Gene Ther. *31*, 808–818.

5. Hordeaux, J., Hinderer, C., Goode, T., Katz, N., Buza, E.L., Bell, P., Calcedo, R., Richman, L.K., and Wilson, J.M. (2018). Toxicology study of intra-cisterna magna adeno-associated virus 9 expressing human alpha-L-Iduronidase in Rhesus Macaques. Mol. Ther. Methods Clin. Dev. *10*, 79–88.

6. Hordeaux, J., Hinderer, C., Goode, T., Buza, E.L., Bell, P., Calcedo, R., Richman, L.K., and Wilson, J.M. (2018). Toxicology study of intra-cisterna magna adeno-associated virus 9 expressing Iduronate-2-sulfatase in Rhesus Macaques. Mol. Ther. Methods Clin. Dev. *10*, 68–78.

7. Hinderer, C., Katz, N., Buza, E.L., Dyer, C., Goode, T., Bell, P., Richman, L.K., and Wilson, J.M. (2018). Severe toxicity in nonhuman primates and piglets following high-dose Intravenous administration of an adeno-associated virus vector expressing human SMN. Hum. Gene Ther. *29*, 285–298.

8. Ramsingh, A.I., Gray, S.J., Reilly, A., Koday, M., Bratt, D., Koday, M.T., Murnane, R., Smedley, J., Hu, Y., Messer, A., et al. (2018). Sustained AAV9-mediated expression of a non-self protein in the CNS of non-human primates after immunomodulation. PLoS. One. *13*, e0198154.

9. Meyer, K., Ferraiuolo, L., Schmelzer, L., Braun, L., McGovern, V., Likhite, S., Michels, O., Govoni, A., Fitzgerald, J., Morales, P., et al. (2015). Improving single injection CSF delivery of AAV9-mediated gene therapy for SMA: a dose–response study in Mice and nonhuman primates. Mol. Ther. *23*, 477–487.

10. Hordeaux, J., Hinderer, C., Buza, E.L., Louboutin, J.P., Jahan, T., Bell, P., Chichester, J.A., Tarantal, A.F., and Wilson, J.M. (2019). Safe and sustained expression of human Iduronidase after intrathecal administration of adeno-associated virus serotype 9 in infant Rhesus monkeys. Hum. Gene Ther. *30*, 957–966.

11. Kumbhare, D., Robinson, L., and Buschbacher, R. (2015). In Buschbacher's Manual of Nerve Conduction Studies, 3rd (Demosmedical).

12. Xiong, W., Wu, D.M., Xue, Y., Wang, S.K., Chung, M.J., Ji, X., Rana, P., Zhao, S.R., Mai, S., and Cepko, C.L. (2019). Regulatory sequences are correlated with ocular toxicity. Proc. Natl. Acad. Sci. U S A *116*, 5785–5794.

13. Shao, W., Shao, W., Earley, L.F., Chai, Z., Chen, X., Sun, J., He, T., Deng, M., Hirsch, M.L., Ting, J., et al. (2018). Double-stranded RNA innate immune response activation from long-term adeno-associated virus vector transduction. JCI. Insight. *3*, e120474.

14. Rosenberg, J.B., Chen, A., De, B.P., Dyke, J., Ballon, D., Monette, S., Arbona, R.R., Kaminsky, S.M., Crystal, R.G., and Sondhi, D. (2020). Safety of direct intraparenchymal AAVrh.10-mediated CNS gene therapy for Metachromatic leukodystrophy. Hum. Gene. Ther. *32*, 563–580.

15. Samaranch, L., Sebastian, W.S., Kells, A.P., Salegio, E.A., Heller, G., Bringas, J.R., Pivirotto, P., DeArmond, S., Forsayeth, J., and Bankiewicz, K.S. (2014). AAV9-mediated expression of a non-self protein in nonhuman primate central nervous system triggers widespread neuroinflammation driven by antigen-presenting cell transduction. Mol. Ther. *22*, 329–337.

16. DaSilva, J.K., and Arezzo, J.C. (2020). Use of nerve conduction assessments to evaluate drug-induced peripheral neuropathy in nonclinical species-A brief review. Toxicol. Pathol. *48*, 71–77.

17. Pardo, I.D., Rao, D.B., Butt, M.T., Jortner, B.S., Valentine, W.M., Arezzo, J., Sharma, A.K., and Bolon, B. (2018). Toxicologic pathology of the peripheral nervous system (PNS): overview, challenges, and current practices. Toxicol. Pathol. *46*, 1028–1036.

18. Lakritz, J.R., Lakritz, J.R., Robinson, J.A., Polydefkis, M.J., Miller, A.D., Burdo, T.H., Robinson, J.A., Polydefkis, M.J., Miller, A.D., and Burdo, T.H. (2015). Loss of intraepidermal nerve fiber density during SIV peripheral neuropathy is mediated by monocyte activation and elevated monocyte chemotactic proteins. J. Neuroinflammation. *12*, 237.

19. Field, A.S., Samsonov, A., Alexander, A.L., Mossahebi, P., and Duncan, I.D. (2019). Conventional and quantitative MRI in a novel feline model of demyelination and endogenous remyelination. J. Magn. Reson. Imaging *49*, 1304–1311.

20. Eguchi, Y., Ohtori, S., Orita, S., Kamoda, H., Arai, G., Ishikawa, T., Miyagi, M., Inoue, G., Suzuki, M., Masuda, Y., et al. (2011). Quantitative evaluation and visualization of lumbar foraminal nerve root entrapment by using diffusion tensor imaging: preliminary results. Am. J. Neuroradiol. *32*, 1824–1829.

21. Horsfield, M.A., and Jones, D.K. (2002). Applications of diffusion-weighted and diffusion tensor MRI to white matter diseases - a review. NMR. Biomed. *15*, 570–577.

22. Diamanti, L., Alfonsi, E., Ferraro, O.E., Cereda, C., Pansarasa, O., Bastianello, S., and Pichiecchio, A. (2018). A pilot study assessing T1-weighted muscle MRI in amyotrophic lateral sclerosis (ALS). Skeletal. Radiol. *48*, 569–575.

23. Fleckenstein, J.L., Watumull, D., Conner, K.E., Ezaki, M., Greenlee, R.G., Bryan, W.W., Chason, D.P., Parkey, R.W., Peshock, R.M., and Purdy, P.D. (1993). Denervated human skeletal muscle: MR imaging evaluation. Radiology *187*, 213–218.

24. Murphy, W., Totty, W., and Carroll, J. (1986). MRI of normal and pathologic skeletal muscle. AJR. Am. J. Roentgenol. *146*, 565–574.

25. Mueller, C., Berry, J.D., McKenna-Yasek, D.M., Gernoux, G., Owegi, M.A., Pothier, L.M., Douthwright, C.L., Gelevski, D., Luppino, S.D., Blackwood, M., et al. (2020). SOD1 suppression with adeno-associated virus and MicroRNA in familial ALS. N. Engl. J. Med. Overseas. Ed. *383*, 151–158.

26. Giugliani, R., Escolar, M., Ficicioglu, C., Harmatz, P., Nevoret, M.L., Cho, Y., Phillips, D., and Falabella, P. (2021). 215. RGX-121 gene therapy for the treatment of severe Mucopolysaccharidosis type II: Interim analysis of the first in human study. Mol. Ther. *29*, 112–113.

27. Mendell, J.R., Al-Zaidy, S.A., Lehman, K.J., McColly, M., Lowes, L.P., Alfano, L.N., Reash, N.F., Iammarino, M.A., Church, K.R., Kleyn, A., et al. (2021). Five-year extension results of the phase 1 START trial of onasemnogene abeparvovec in spinal muscular atrophy. JAMA Neurol. *78*, 834–841.

28. Day, J.W., Finkel, R.S., Chiriboga, C.A., Connolly, A.M., Crawford, T.O., Darras, B.T., Iannaccone, S.T., Kuntz, N.L., Peña, L.D.M., Shieh, P.B., et al. (2021). Onasemnogene abeparvovec gene therapy for symptomatic infantile-onset spinal muscular atrophy in patients with two copies of SMN2 (STR1VE): an open-label, single-arm, multicentre, phase 3 trial. Lancet Neurol. *20*, 284–293.

29. Qu, W., Wang, M., Wu, Y., and Xu, R. (2015). Scalable downstream strategies for purification of recombinant adeno- associated virus vectors in light of the properties. Curr. Pharm. Biotechnol. *16*, 684–695.

30. Rieser, R., Koch, J., Faccioli, G., Richter, K., Menzen, T., Biel, M., Winter, G., and Michalakis, S. (2021). Comparison of different liquid chromatography-based purification strategies for adeno-associated virus vectors. Pharmaceutics *13*, 748.